Measuring fluctuating dynamics of sparsely crosslinked actin gels with dual-feedback nonlinear microrheology

Kenji Nishizawa, Natsuki Honda, Shono Inokuchi, Hiroyuki Ebata, Takayuki Ariga, and Daisuke Mizuno

Measuring fluctuating dynamics of sparsely crosslinked actin gels
with dual-feedback nonlinear microrheology

Kenji Nishizawa, ‡[b] Natsuki Honda, ‡[a] Shono Inokuchi,[a] Hiroyuki Ebata,[a] Takayuki Ariga[c] and Daisuke Mizuno*[a]

We investigate the fluctuating dynamics of colloidal particles in weakly crosslinked F-actin networks with optical-trap-based microrheology. Using the dual-feedback technology, embedded colloidal particles were stably forced beyond the linear regime in a manner that does not suppress spontaneous fluctuations of particles. Upon forcing, a particle that was stably confined in a cage made of the network's crosslinks started to intermittently jump to the next caging microenvironments. By investigating the statistics of the jump dynamics, we discuss how heterogeneous relaxations observed in equilibrium systems become homogeneous when similar jumps were activated under constant forcing beyond the linear regime.

I INTRODUCTION

Actin filament (F-actin) networks are the major component of cytoskeletons that regulate various cellular processes [1]. The mechanical properties of cytoskeletons have been intensively investigated since they control proper biological functions [2-7]. F-actin networks are typical soft materials in the sense that their physical properties are determined by mesoscale (nm ~ μm) structures and their fluctuating dynamics. To elucidate the mechanical properties, the thermal fluctuation of colloidal particles embedded in entangled F-actin networks has been measured with a technique referred to as linear microrheology (MR).

MR is a technique to probe local mechanical properties of a sample from the movement of embedded probe particles [5,8-13]. Linear MR observes either a probe's spontaneous fluctuation (Passive MR: PMR) [5,9,14] or its response to small external forces (Active MR: AMR) [10,11,15]. At thermodynamic equilibrium, the fluctuation-dissipation theorem (FDT) guarantees that AMR and PMR provide equivalent information, *i.e.*, the linear viscoelasticity of surrounding medium [10,16,17]. For nonlinear MR, probe particles are forced beyond the linear regime. In ordinary nonlinear MR, a direct response of the probe movement to the force was investigated in a similar way to AMR (nonlinear AMR) [18-20]. Among these techniques, linear PMR has been widely used to investigate soft materials, including F-actin networks.

The F-actin network is characterized by a persistence length of ~10 μm and a diameter of 7 nm [1]. The meshwork size of the network is typically 100 nm to sub-μm when polymerized at physiologically relevant concentrations (~ mg/mL) [21]. For a crosslinked network, the crosslink distance l_c falls somewhere between the mesh size and the contour length of the actin filament. In semi-dilute or non-crosslinked conditions, the mesoscale structures fluctuate spontaneously with thermal energy. By observing the thermal fluctuation with linear PMR, the anomalous properties of F-actin networks, *e.g.*, non-Gaussian statistics [22-24] and sub-diffusive power-law dynamics [2,4,6], have been studied. Even though the radius a of the probe particle was sufficiently greater than ξ, the fluctuation showed a violation of Stokes' law, indicating that the continuum assumption does not hold [2,4].

When a probe particle is made smaller, the dynamics dramatically change at $\xi \sim a$; the particle starts to jump between different local cages infrequently. The temporal distribution of these jumps results in the anomalous sub-diffusion [6,22,23], likely reflecting the heterogeneity of microscale structures. Thermal jumps become rare to observe when the F-actin concentration is increased or the network is crosslinked. In that case, by forcing the probe particle beyond its linear response regime, not only the direct response to the force but the stochastic fluctuation is also produced. Such non-thermal fluctuation is expected to provide abundant useful information to investigate physical properties of non-equilibrium systems. However, observing the "purely" stochastic fluctuation induced under nonlinear forcing has been challenging.

MR experiments can be performed with high bandwidth and high precision by utilizing the optical−trapping and the laser-interferometry technique [5,8,9]. In ordinary nonlinear MR experiments, a colloidal particle was trapped with a fixed drive laser, and the piezo-mechanical stage holding the sample container was moved [20]. The probe particle's position within the trap was measured via the diffraction of a probe laser that

impinges on the particle (the back-focal-plane interferometry: BFPI [25]). The optical-trapping force then fluctuated according to the stochastic motion of the particle within the trap. Furthermore, the probe fluctuation was suppressed by the trapping potential formed around the laser focus [10,26]. These artifacts critically hinder our aim to investigate the fluctuating dynamics of a probe particle under nonlinear forcing.

In this study, we investigate the non-thermal fluctuation which was induced under constant forcing beyond the linear response regime (nonlinear PMR). We introduced a fast feedback control of the drive laser, referred to as *force feedback*. The real-time position of the probe particle was measured with BFPI, and the position (focus) of the drive laser was rapidly optimized so that it quickly followed the fluctuating probe particle. Thereby, the well-controlled force was applied to the probe particle without preventing its fluctuation. In order to track a vigorously-fluctuating probe particle over large distances, we introduced another feedback referred to as *stage feedbac*k [27]. A piezo-mechanical stage on which the sample chamber was placed was also controlled by feedback. Thereby, the fluctuating probe particle was stably kept close to the focus of a fixed probe laser.

Using the dual-feedback technique, nonlinear PMR was performed in loosely crosslinked F-actin gels. Forces of up to several pN caused directed movements of the probe, not a continuous smooth movement like in homogeneous liquids, but with intermittent hops that occurred randomly both in time and size. Despite the apparent heterogeneity implied by the observation, careful statistical analysis showed that the underlying energy landscape was *homogeneously* stochastic. These findings highlight the potential of the developed technique to investigate a nonlinear and dynamic response in a nonequilibrium soft matter.

II MATERIALS

Globular (G-) actin was prepared from rabbit skeletal muscle according to a standard protocol [3] and was stored at -80 ℃ in G-buffer [2 mM tris-Cl, 0.2 mM $CaCl_2$, 0.5 mM dithiothreitol (DTT), and 0.2 mM ATP (pH 7.5)]. G-actin was diluted into F-buffer [1 mM Na2ATP, 2 mM HEPES, 1 mM EGTA, 2 mM $MgCl_2$, and 50 mM KCl (pH 7.5)] to initiate actin polymerization. To prepare a crosslinked F-actin gel, G-actin, heavy meromyosin (HMM, Cytoskeleton Inc., USA), and a small number of polystyrene beads (Polysciences Inc., $2a = 1\,\mu m$) were mixed. The final concentration of G-actin and HMM were 1.3 mg/ml and 0.04 mg/ml, respectively. The solution was then quickly infused into sample chambers made of a microscopic glass slide (size 7.6 × 2.6 cm; Matsunami Glass Ind., Ltd., Japan) and a No.1 coverslip (size 26 mm × 10 mm × 150 μm; Matsunami Glass) placed on two parallel layers of double-sided tape. Samples were left for polymerization for at least 1 h.

III NONLINEAR PMR

As shown in Fig. 1a, two lasers were used to conduct the force and stage feedback. The optical trapping force $F(t)$ was applied to a probe particle with a drive laser ($\lambda = 1064\,nm$, 4 W CW, Nd:YVO4, Compass, Coherent Inc.). The focus position of the drive laser was rapidly steered by an acousto-optic deflector (AOD, model DTSX-400-1064, AA Opto-Electronic). The position of the drive laser was measured with BFPI by using a quadrant photodiode (QPD) placed at the back-focal plane of the objective and condenser lenses. QPD provided a voltage signal $V(t)$ proportional to the separation between the laser focus and the center of the probe particle. As written below, the optical-trapping force was then tuned to the desired quantity by the force feedback.

We define displacements $u(t)$, $u_{AOD}(t)$, and $u_d(t)$ as shown in Fig. 1b. $u(t)$ and $u_{AOD}(t)$ are the displacements of the probe particle and the focus of the laser, respectively. $u_d(t)$ is the distance between the probe particle and the focus of the laser. The displacement of the probe in the sample is described as $u(t) = u_{AOD}(t) - u_d(t)$. As shown in Fig. 1a, the output voltage $V(t)$ of the QPD, which is proportional to $u_d(t)$, was fed to a Proportional-Integral-Derivative (PID) controller (SIM960, Stanford Research Systems). An output signal $\varepsilon_{AOD}(t)$ from the PID controller was produced via the integral term of the PID, $\varepsilon_{AOD}(t) = I \int \{V(t) - s_0\}\, dt$, where I is the programmable feedback gain and s_0 is the set point of the PID controller. Since the laser moves by $u_{AOD}(t) = C_{AOD}\varepsilon_{AOD}(t)$, $u_{AOD}(t)$ and $u_d(t)$ are correlated via the feedback as,

$$u_{AOD}(t) = C_{AOD}\varepsilon_{AOD}(t) = (1/\tau_{PID}) \int \{u_d(t) - C_d s_0\} dt.$$

(1)

Here, $\tau_{PID} \equiv C_d / C_{AOD} I$ is a characteristic response time of the force-feedback system. The proportionality constants, $C_d \equiv u_d(t)/V(t)$ and $C_{AOD} \equiv u_{AOD}(t)/\varepsilon_{AOD}(t)$, were obtained following procedures given in Refs. [10,27]. The fluctuation slower than τ_{PID} is tracked by laser focus as $u_{AOD}(t)$, while the probe's fluctuation faster than τ_{PID} is detected by QPD as $u_d(t)$. To ensure that the optical manipulation does not suppress the particle's intrinsic fluctuations, we adjusted τ_{PID} to be smaller than the response time of the trapped particle, $\tau_c \equiv \gamma_0 / k \sim 0.03\,s$, by changing the programmable feedback gain I. In our experiment, we used τ_{PID}: $7.7 \times 10^{-6}\,s$. The distance between the probe particle and the focus of the drive laser is then kept constant at $u_d = C_d s_0$ (Fig. 1b). The constant force $F = k_d u_d$ is then applied to the probe particle, regardless of its fluctuating movements.

For nonlinear MR, the applied force induces vigorous probe fluctuations and drifts. Force-feedback MR cannot be precisely conducted when the AOD-controlled laser ($\lambda = 1064\,nm$) moves away from the optical axis of the objective lens. An offset in QPD output and an error in the
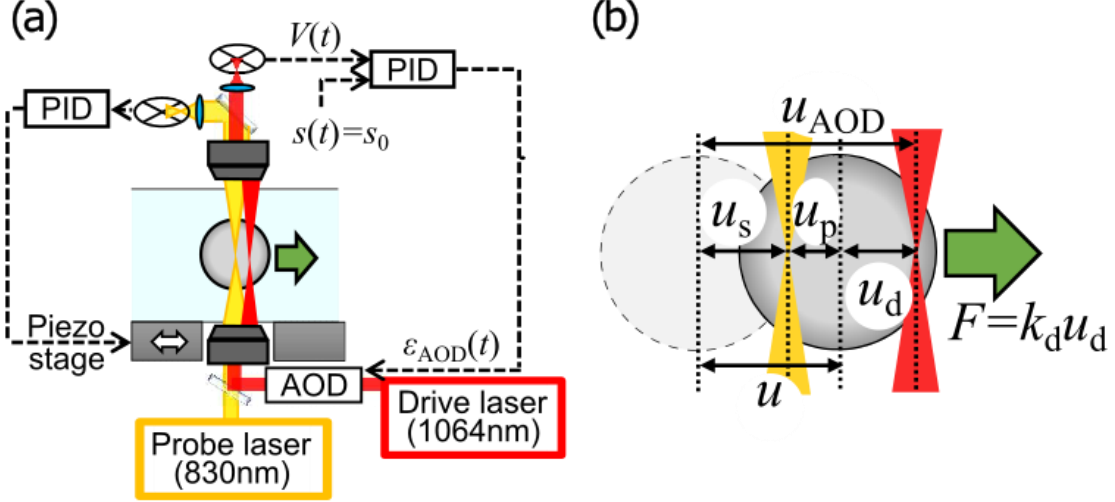
FIG. 1. Nonlinear MR under dual feedback. (a) Schematic of the setup for dual-feedback nonlinear MR. Force-feedback control (right loop) and stage feedback control (left loop) are carried out simultaneously. For force feedback, a constant offset $s(t) = s_0$ was fed to the set point of the PID controller to keep a constant distance between the center of the fluctuating probe particle and the drive laser, u_d. For stage feedback, the displacement of the piezo stage u_s was controlled to locate the probe particle around the focus of the fixed probe laser. (b) u_d was maintained by force-feedback control. A stable, constant force $F = k_d u_d$ was applied to the probe in one direction. The total displacement of the probe u was obtained by summing u_p and u_s.

calibration factor C_d appear when the laser is far (~10 μm) from the optical axis (see Appendix A for the details). Also, the force feedback follows the probe particle only in lateral directions; deviation of the probe from the laser focus along the optical axis can also introduce significant errors due to the change of the BFPI sensitivity [28]. In order to track a largely fluctuating probe [29], another feedback control mechanism referred to as *stage feedback* [27] was introduced in addition to the force feedback.

As detailed in our prior study [27], stage feedback was applied in three dimensions (3D) by controlling the piezo stage on which a sample chamber was placed (Fig. 1a) [27]. The probe displacements in lateral (*x*-, *y*-) directions were measured by BFPI using another fixed probe laser (λ = 830 nm, 150 mW, IQ1C140, Power technology Inc.); displacements in the axial (*z*-) direction were measured by analyzing the pattern of the microscope image of the probe particle [28]. The piezo stage was then controlled using PID feedback. Since the probe laser was weak and the set point for the stage feedback was set to zero, the optical-trapping force applied by the probe laser was negligible. Since the response of a piezo stage is slow due to its inertia, the feedback-response time was set much larger than the force feedback. This stage feedback can be performed within the travel range of the piezo stage, ~200 μm in this study.

Performing the force feedback and stage feedback simultaneously (referred to as the dual-feedback mode), stage feedback keeps the particle close to the optical axis (Fig. 1a).

The displacement of the probe $u(t)$ is obtained from the sum of the displacement of the piezo stage $u_s(t)$ and the distance between the probe particle and the focus of the probe laser $u_p(t)$, $u(t) = u_p(t) + u_s(t)$. The piezo stage tracks the slow/large fluctuations of the probe $u_s(t)$, while the fast/small fluctuations are detected by the BFPI using the probe laser $u_p(t)$. Because of the extensive dynamic range and high resolution, this method is suitable for observing the fluctuating dynamics of the probe particle driven by nonlinear forcing.

IV RESULTS

Using the technique described above, a $2a$ = 2 μm colloidal particle (Silica, Polysciences) was pulled in F-actin gels that were sparsely crosslinked with heavy meromyosin (F-actin 1.3 mg/mL and HMM 0.04 mg/mL). Fig. 2a shows the displacements of the probe particles in the direction of the force. The probe particles were trapped in the surrounding gel [16] when the applied force was small (*e.g.*, F = 1.0 pN *yellow line*, and F = 2.5 pN *green line*), guaranteeing that thermal reptation does not occur. The power spectral density (PSD) of the probe displacements scaled as $PSD \cdot \omega / 2k_B T$ (ω: angular frequency) was not affected by the application of such small forces (Fig. 2b). At F = 3.4 pN, however, some probe particles started to move with intermittent jumps (*blue curves* in Fig. 2a which correspond to *blue broken curve* in Fig. 2b). When these intermittent jumps were not observed, the PSD slightly decreased at low frequencies (Fig. 2b, *blue solid curve*), which
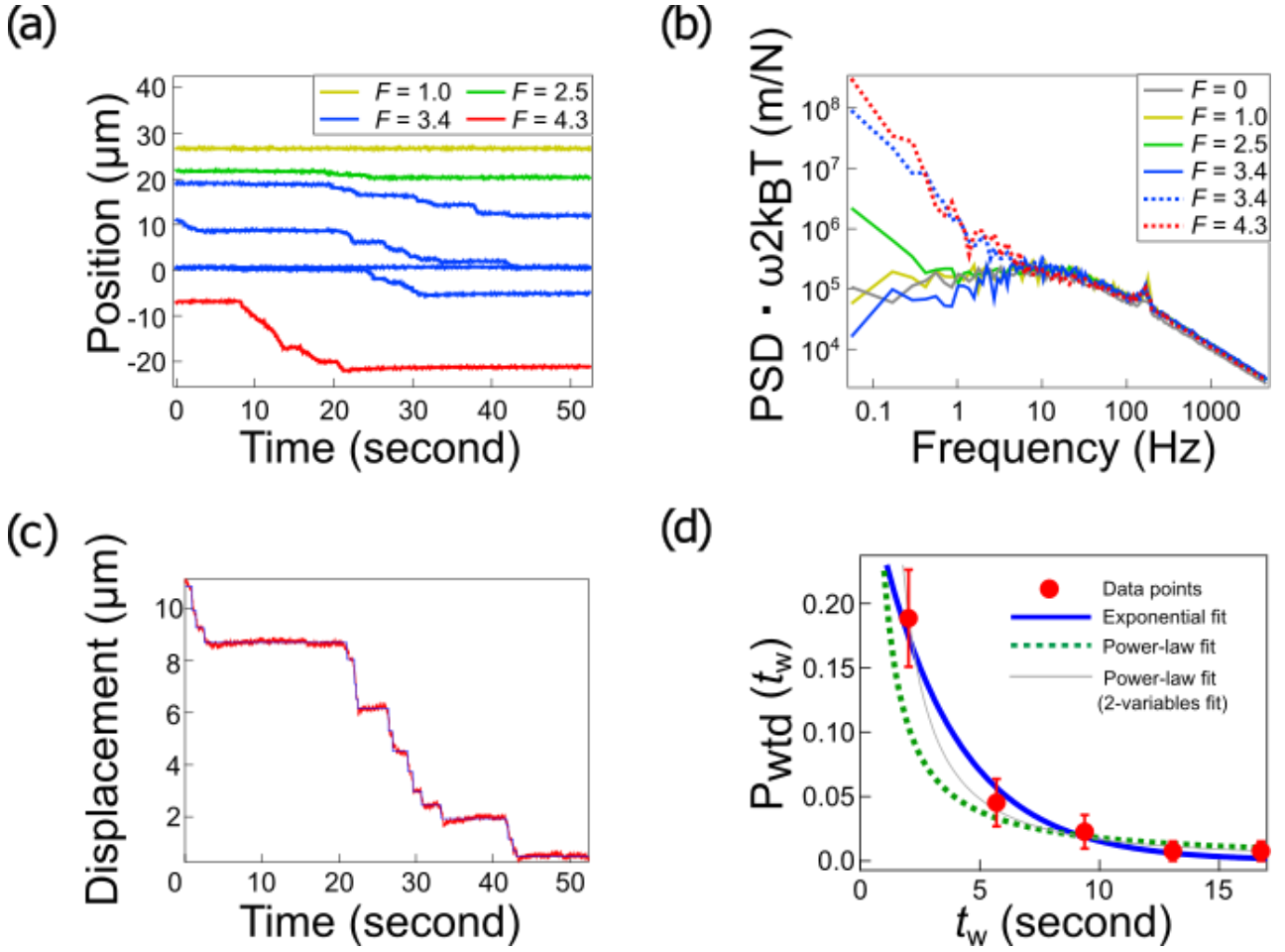
FIG. 2. (a) Time series of the probe movements in a crosslinked F-actin gel under constant forcing F. Nonlinear force-clamp MR was conducted with τ_{PID}: 7.7×10^{-6} s, $k_d \sim 1.7 \times 10^{-5}$ N/m and $k_p \sim 1.5 \times 10^{-5}$ N/m. Intermittent jumps were observed when the applied force was increased ($F = 3.4$ pN: *blue curve*, $F = 4.3$ pN: *red curve*). (b) PSD$\cdot\omega/2k_BT$ obtained by force-clamp MR at different constant forces. These appeared in the PSD as enhanced non-thermal fluctuations at low frequencies (*broken curves*). (c) Probe movements under constant forcing 3.4 pN (*red line*). *Blue line* is the fit used to extract jumps of the probe using a step detection algorithm. (d) Probability distribution $P_{wtd}(t_w)$ of the waiting times between consecutive jumps (*red circles*), and bars indicate the normalized square root of the count which corresponds to the standard deviation. The results were fit by an exponential function $P_{wtd}(t_w) = \exp(-At_w)/N_e$ (*blue solid curve*), power-law $P_{wtd}(t_w) = t_w^{-\alpha}/N_p$ (*green broken curve*, $\alpha = 1.10$) and two-parameter power-law function $P_{wtd}(t_w) = B\,t_w^{-\alpha}$ (*gray thin curve*, $\alpha = 1.52$). N_e and N_p are the normalization factors given as $\int_{min}^{max} \exp(-At_w)dt_w$, $\int_{min}^{max} t_w^{-\alpha}dt_w$ where min = 0.175 and max = 18.6 are the minimum and maximum of t_w observed.

is consistent with the stress stiffening of cytoskeletal gels [30,31]. All probe particles experienced intermittent jumps when the applied force was increased further ($F = 4.3$ pN, *red curve* in Fig. 2a). The directed movements via intermittent jumps increased fluctuations at low frequencies, whereas fluctuations at high frequencies were not changed (Fig. 2b).

Similar behavior has been frequently observed in various non-equilibrium systems [16,32]; the increased fluctuations at low frequencies can be attributed to non-thermal fluctuations generated by energy input, provided here by the drive laser (*broken curves* in Fig. 2b).
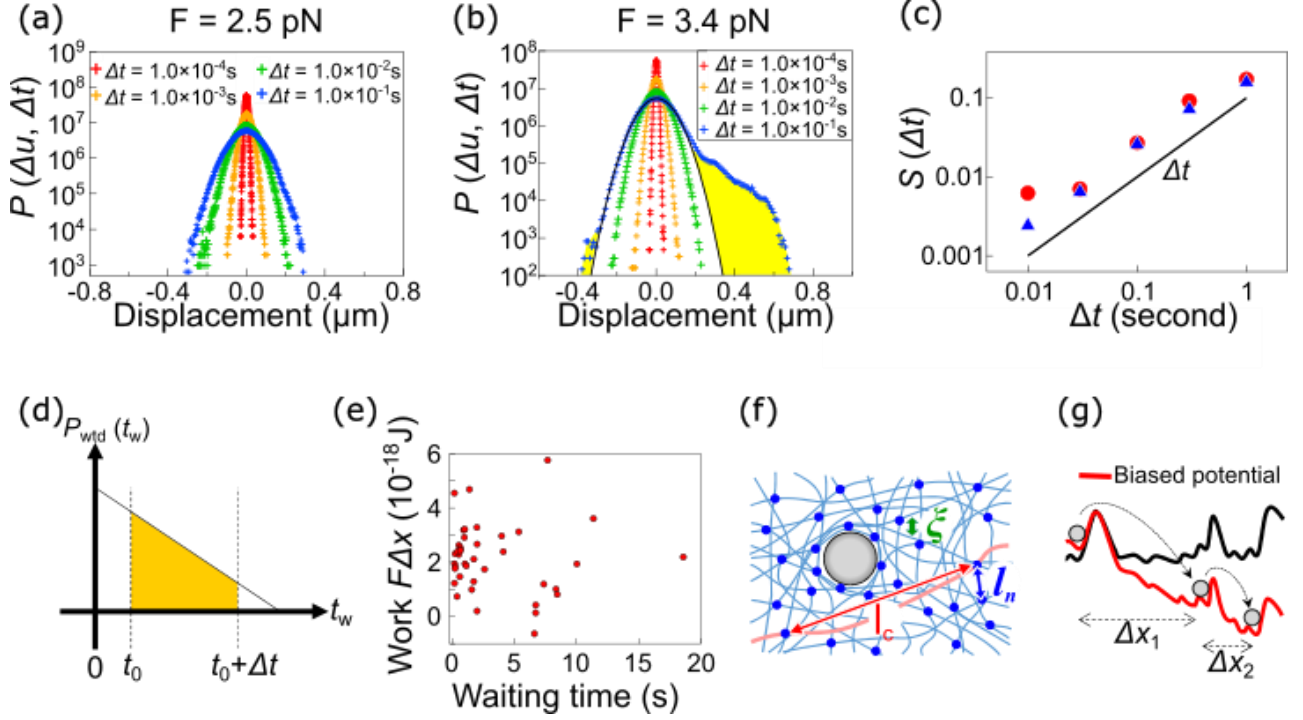
FIG. 3. (a) The probability distribution $P(\Delta u, \Delta t)$ of probe displacements Δu in duration Δt. A constant force ($F = 2.5$ pN) was applied to the probe in a positive direction. (b) $P(\Delta u, \Delta t)$ measured at $F = 3.4$ pN. The central portion of the distribution ($\Delta t = 0.1$ s) was fit with a Gaussian (*black curve*). The area of the yellow region $S(\Delta t)$ was obtained by subtracting the Gaussian from the total fluctuations. (c) $S(\Delta t)$ plotted as a function of the lag time 0.01 s $\leq \Delta t \leq 1$ s (circle: $F = 4.3$ pN, triangle: $F = 3.4$ pN). (d) A schematic describing the relation between $S(\Delta t)$ and $P_{\mathrm{wtd}}(t)$. Provided that the last jump took place at $t = 0$, the area colored in orange indicates $S(\Delta t)$. (e) Scatter plot of work $F\Delta x$ and waiting time t_{w} taken before the jump event. The tracer beads in a crosslinked F-actin gel were under constant forcing $F = 3.4$ pN (Fig. 2c). (f) Schematic describing the characteristic lengths of crosslinked actin: network's mesh size ξ (~ 140 nm), the distance between crosslinks along the same filament l_{c} (~ 7 μm), the distance between nearest crosslinks l_{n} (~ 0.5 μm). *Blue circles* are crosslinks. (g) Schematic describing jumping of probe particle to neighbouring potential wells, which are biased by the applied force (*red curve*). Jumping does not show glassy heterogeneous dynamics since the probe bead is not trapped in shallow sub-basins in the original potential wells (*black curve*).

The dynamics of the stochastic jumps were investigated with the probability distribution $P_{\mathrm{wtd}}(t_{\mathrm{w}})$ of the waiting times t_{w} between consecutive jumps. Jump events in the trajectory of the probe (Fig. 2c) were detected using the step detection algorithm. We chose the algorithm in which the step size for each jump is an adjustable parameter [33]. $P_{\mathrm{wtd}}(t_{\mathrm{w}})$ of the forced jumps is shown in Fig. 2d. The experimental results were fitted by single-parameter functions, *i.e.*, the exponential $P_{\mathrm{wtd}}(t_{\mathrm{w}}) \propto \exp(-At_{\mathrm{w}})$ (*solid blue curve* in Fig. 2d) and the power-law function $P_{\mathrm{wtd}}(t_{\mathrm{w}}) \propto t_{\mathrm{w}}^{-\alpha}$ (*broken green curve* in Fig. 2d). Since the $P_{\mathrm{wtd}}(t_{\mathrm{w}})$ data is normalized in Fig. 2d, the functions were also normalized in the range between the minimum (0.175s) and the maximum (18.6s) of waiting times observed in the experiments. The weighted residual sum of squares, *i.e.*, $\chi^2 = \sum_i \{(y - y_i)/w_i\}^2$ where y is a fitted value for a given point, y_i is the original data value and w_i is the wight proportional to $y_i^{1/2}$, shows that the exponential function ($\chi^2 = 1.22$) fits better than the power-law one-variable fitting ($\chi^2 = 6.21$). If $P_{\mathrm{wtd}}(t_{\mathrm{w}})$ is fitted by a two-parameter power-law function $P_{\mathrm{wtd}}(t_{\mathrm{w}}) = C t_{\mathrm{w}}^{-\alpha}$ (*gray thin curve* in Fig. 2d), $\chi^2 = 0.44$ was slightly smaller than the one-parameter exponential function fitting. However, the Akaike Information Criterion (AIC), which is used to test the validity of the fitting, indicated that the two-variable power-law function was overfitting (AIC

= 10.44) compared to the exponential function fitting (AIC = 4.55) and the power-law one-variable fitting (AIC = 9.54) [34,35]. The *blue solid curve* shows the exponential fitting for $P_{wtd}(t_w)$, indicating that each jump occurs following Poissonian statistics and that the forced probe particles exhibited Markov jumps that occurred randomly in time. However, this is a fit to experimental data measured within a short waiting time range, and it is not clear enough to make a strong statement that the particles exhibit Markov jumps only from this fitting.

Therefore, the dynamics of the forced probe particle were investigated with another approach that does not need to guess when the actual jumps occur. We calculated the probability distribution $P(\Delta u, \Delta t)$ of the probe displacements Δu in the direction of the applied force that occurred during a lag time Δt, referred to as van Hove distributions. For weak forcing ($F \leq 2.5$ pN), the shape of $P(\Delta u, \Delta t)$ did not evolve with Δt and remained Gaussian (Fig. 3a). For stronger forcing ($F = 4.3$ pN, Fig. 3b), the distribution function was close to Gaussian only when the lag time Δt was small. As the lag time Δt increases, the tail of the distribution extends in the direction of the force ($\Delta u > 0$). In contrast, the distribution in the opposite direction is hardly affected, remaining Gaussian.

Non-Gaussian tails have been frequently observed when a probe exhibits rare but large jumps [29]. In such a case, the area $S(\Delta t)$ exceeding the thermal Gaussian distribution (the yellow region in Fig. 3b) indicates the probability that at least one jump occurred in Δt . The distribution of thermal fluctuations was estimated by fitting the Gaussian function to the central portion of the van Hove distribution, as shown in Fig. 3b. By subtracting the integrated probability of thermal fluctuations from the total, the area of the yellow region [$S(\Delta t)$] in Fig. 3b was obtained. Fig. 3c indicates that $S(\Delta t)$ evolves linearly with Δt . Note that $S(\Delta t)$ is related to $P_{wtd}(t_w)$ by

$$S(\Delta t) \propto \int_0^\infty dt_0 \int_{t_0}^{t_0+\Delta t} P_{wtd}(t_w)dt_w , \qquad (2)$$

as schematically shown in Fig. 3d. $S(\Delta t)$ can then be expressed as $S(\Delta t) \propto -\exp(-A\Delta t)+1$ from $P_{wtd}(t_w) \propto \exp(-At_w)$, consistent with the experimental result shown in Fig. 3c when Δt is small. It indicates that $S(\Delta t)$ obeys Markov-like Poissonian behaviour with independent jump evens.

As an additional examination, we considered the potential scenario where jumps do not adhere to a Poisson distribution. Upon performing a single-parameter fitting for $P_{wtd}(t_w)$, we found that the exponential function provided a superior fit compared to the power-law function (Fig. 2d). If we were to presume that the two-parameter power-law fitting could describe the jumps as $P_{wtd}(t_w) = C t_w^{-\alpha}$ with $\alpha = 1.52$,

$S(\Delta t) \propto \Delta t^{2-\alpha} \approx \Delta t^{0.48}$ is derived by following Eq. (2), which did not conform well to the data shown in Fig. 3C. These inconsistencies can be resolved by rejecting the power-law assumption, thus supporting the Poissonian dynamics. We also examined the work done by the external force during the jumps ($F\Delta x$) and the waiting time before the jump (t_w) (Fig. 3e). The result shows that these two do not correlate, which also supports that the jumping dynamics obeys Poissonian.

V DISCUSSION

In order to have insight into the observed probe dynamics, it is necessary to estimate the characteristic lengths of our F-actin sample. The mesh size ξ of the semi-flexible network is obtained from the length density $\rho (= 49 \ \mu m^{-2})$ of the filaments as ξ : $1/\sqrt{\rho} \sim 140$ nm [21]. The average distance l_c between crosslinks along each F-actin filament is estimated as

$$l_c \sim (6\rho k_B T l_p^2 /G)^{1/3}, \qquad (3)$$

where $l_p = 10 \ \mu m$ is the persistent length of actin filaments without phalloidin labeling. G is the elastic plateau modulus of F-actin / HMM gels that were not subjected to external forces [36]. We then obtain $l_c \sim 7 \ \mu m$ whereas the average distance between nearest crosslinks is $l_n \sim \sqrt[3]{\xi^2 l_c}$: 0.5 μm since the number of cross-linkers in the unit volume is estimated to be $(\xi^2 l_c)^{-1}$ in the semi-flexible polymer (Fig. 3f) [37,38]. These characteristic length scales of the F-actin gel (mesh size ξ, persistent length l_p, the crosslink distance l_c) are similar to the size of the probe particle ($a = 1 \ \mu m$) in order of magnitude, and therefore could profoundly affect the fluctuating dynamics of the probe particles.

Without external forcing, probe particles are deeply constrained in the potential wells formed by the elastic microenvironments of the crosslinked gel. Therefore, thermal fluctuations could reflect merely the bottom curvature of the potential. The Gaussian nature (Fig. 3a) of the distribution under $F = 2.5$ pN implies that the medium surrounding the probe is regarded as a homogeneous continuum as far as linear MR is concerned. This is likely because our probes are constrained in the network with ξ smaller than the probe size. On the other hand, the jump process observed under nonlinear forcing ($F \geq 3.4$ pN) may reflect the whole depth of the potential associated with sparse crosslinks rather than the mesh of the network. Even if $l_n < a$, the position of filaments and crosslinks can rearrange to allow probe jumping. It is not necessary to break the network structure as long as $l_c > a$. It is also to be noted that the ~ pN forces applied in this study are not enough to break the actin filaments or the HMM crosslinks. When the distance between nearest crosslinks l_n is sufficiently smaller than the particle size $2a$, the force applied through the particle induces a nonlinear response of the network and relaxation of the sample [30,39-42]. In our study, where the

distance between nearest crosslinks l_n is comparable to the particle size, when the force applied to the particles is increased, the fluctuations of the particles do not decrease in any frequency range (Fig. 2b), suggesting that the particles stochastically transition to the next potential without applying enough force for the filaments to exhibit a nonlinear response (Fig. 3g).

It has been reported that probe particles in dilute (ξ : a) and non-crosslinked F-actin networks jump intermittently and spontaneously in the absence of any external force [6,22]. Such thermal jumps also showed non-Gaussian dynamics with side tails in the van Hove distributions. However, the waiting-time distribution of the thermal jumping followed a power-law function, $P_{wtd}(t) \propto 1/t^\alpha$ ($1 < \alpha < 2$) [6,22], in contrast to the forced jumps observed in this study. It was reported that the observed power-law distribution is consistent with the theoretical model for anomalous diffusion: a continuous time random walk (CTRW) whose waiting times have a distribution with a power-law decaying tail [43]. Bouchaud's trap model [44-46] links the power-law distribution of waiting times to the heterogeneity of microenvironments, leading to sub-diffusion. In the widely-accepted phenomenological theory, glassy dynamics are attributed to the probability density of microenvironments $\rho(E)$ having a potential depth E [44]. For instance, in the case of non-crosslinked gels used in the prior study [6,22], the energy landscape should contain small basins whose depth is broadly distributed. The probe particle was temporarily trapped in such basins. Since thermal probes free from forcing are trapped longer in deeper potentials following Boltzmann's statistics, a power-law distribution of waiting times $P_{wtd}(t)$ was observed. These prior reports, both experiments and theories, thus indicate the presence of mechanically heterogeneous microenvironments that frequently show up in soft glassy materials [6,22,47].

On the other hand, when a probe particle in a cytoskeletal network was subjected to an optical-trapping force, $P_{wtd}(t)$ showed an exponential decay which is typical of Poisson-Markov jumps. Such dynamics characterized by a single relaxation time indicate that the potential depths provided by different microenvironments are narrowly distributed. In the sparsely crosslinked actin gels prepared in this study, we expect that crosslinks would create global wells which are much deeper than $k_B T$, in addition to the small subbasins as shown in Fig. 3g. Because $l_n < a$, we believe that many crosslinks are involved in forming the global well (Fig. 3f). A probe particle needs to squeeze out from many crosslinks encircling it to hop to the neighboring microenvironment. From the statistical reason, it is reasonable to expect that the threshold energy (depth of the global potential) may not be broadly distributed (Fig. 3g). Note that the external force effectively decreases the potential E by a margin much larger than the thermal energy ($F\Delta x >> k_B T$). Under such strong

forcing, small or intermediate sub-basins in the energy landscape will no longer trap the probe beads (Fig. 3g).

VI CONCLUSION

In this study, we investigated the fluctuating dynamics of colloidal particles transported in crosslinked F-actin gels under the application of the optical-trapping force. By forcing beyond its linear response regime, not only the direct response to the force but the stochastic fluctuation was also produced. The purely stochastic fluctuation was measured while applying an optical-trapping force to the probe particle. In order to conduct this nonlinear PMR experiment, a well-controlled constant force was applied to a probe particle by the rapid feedback control of the trapping laser (force feedback). Another feedback control, the stage-feedback [27], was also performed to track vigorously-fluctuating particles at large distances.

With this dual feedback technique, well-controlled constant forces were applied to probe particles embedded in sparsely crosslinked F-actin networks. Within the linear forcing regime, the probe particle was confined in cage-like microenvironments provided by the sparse crosslink of the gel. The fluctuation under this condition was Gaussian, implying that the continuum assumption seems to work as far as a linear response is concerned. Forcing beyond the linear regime, we observed the jumping of the probe particle to a neighboring cage, indicating the presence of heterogeneous microenvironments. In prior studies, thermal jumping has been observed in similar F-actin networks and other soft materials [6,22,23,48]. The durations for the thermal jumping (waiting times in each site) typically showed power-law distribution, which leads to the sub-diffusive dynamics of probe particles. This power-law distribution of waiting times indicated the presence of heterogeneous microenvironments. On the other hand, the jumping of a forced probe was found to follow Markov step dynamics in this study. This observation indicates that the energy landscape for the activation of forced jumping is homogeneous. We discussed how the dynamics under nonlinear forcing could become homogeneous even if microenvironments are considered heterogeneous.

In living cells, various organelles and vesicles are transported within the meshwork of cytoskeletons by force generated by, *e.g.*, molecular motors. Therefore, the fluctuation in the cytoskeleton under linear and nonlinear forcing relates to the mechanism of intracellular transportation. As we found in this study, the dynamics of the non-thermal fluctuation induced under nonlinear forcing qualitatively differ from those under linear forcing. Note that living organisms are mostly made of soft materials, and the soft materials (including F-actin used here) are typically driven beyond the linear response regime by forces with physiologically relevant magnitude (pN

~ nN). Owing to the nonlinearity, motor-generated forces profoundly modulate the mechanics of living systems, as observed *in vitro* [16,49] and *in vivo* [27,50]. Understanding the dynamics under nonlinear forcing is thus the key to elucidating the physical process of intracellular transportation [50,51]. The experiment presented here demonstrated the potential of nonlinear PMR using our dual-feedback technology by specifically revealing that homogeneous dynamics emerge under nonlinear forcing.

CONFLICTS OF INTEREST

There are no conflicts to declare.

‡ These authors contributed equally to this work.
* Corresponding author: mizuno@phys.kyushu-u.ac.jp

==APPENDIX A: THE SENSITIVITY AND OFFSET ERROR IN BFPI SIGNAL DEPEND ON THE LASER FOCUS POSITION==

In the case of force-feedback MR using a single AOD-controlled laser, the laser could move away from the optical axis during an experiment. Then, the sensitivity $1/C_d$ and offset-error voltage in QPD output V_0 may vary. Therefore, we measured $1/C_d$ and V_0 as a function of the laser deflection by AOD and estimated the errors that may appear during feedback-MR experiments.

Melamine particles with a diameter of 1 µm were trapped in water, and the focus position of the laser was oscillated by AOD as $u_{AOD}(t) = Ae^{-i\omega t} + u_L$, with $A = 71.5$ nm and $\omega/2\pi = 10$ kHz. u_L is the average distance of the laser focus from the optical axis (Fig. 4a). During the experiment, the probe particle was trapped at the position u_L because the oscillation of the laser was much faster than the response time of the probe ($\tau_c = \gamma_0 / k_p$; 7.7 ms). Here, γ_0 is the friction constant of the probe particle and k_p is the trap stiffness of the probe laser. The separation u_d between the laser focus and the probe center was oscillated sinusoidally as $u_d = Ae^{-i\omega t}$. By measuring the QPD output voltage $V(t; u_L) = A/C_d(u_L)e^{-i\omega t} + V_0(u_L)$ with the lock-in amplifier, the sensitivity $1/C_d$ [V/m] was obtained as the ratio between the oscillation amplitudes of $u_{AOD}(t)$ and $V(t; u_L)$. The offset of the QPD output $V_0(u_L)$ was obtained by taking the time average of the QPD output, $V_0(u_L) = \langle V(t; u_L) \rangle$.

In Fig. 4b, the red circles and *blue open triangles* represent the sensitivity ($1/C_d$) and the offset (V_0), respectively. When $|u_L|$ was increased, the sensitivity $1/C_d$ tended to decrease, and the offset error V_0 arose. The laser deflection by the AOD is certified up to 45 mrad by the manufacturer, which corresponds to -10 µm $\leq u_L \leq 25$ µm in our setup. Within the range, $1/C_d$ varied more than 10% and $|V_0|$ exceeded 1 V at large $|u_L|$. When calibrated, $|V_0| \sim 1$ V corresponds to more than 100 nm. BFPI accurately measures the probe displacement when
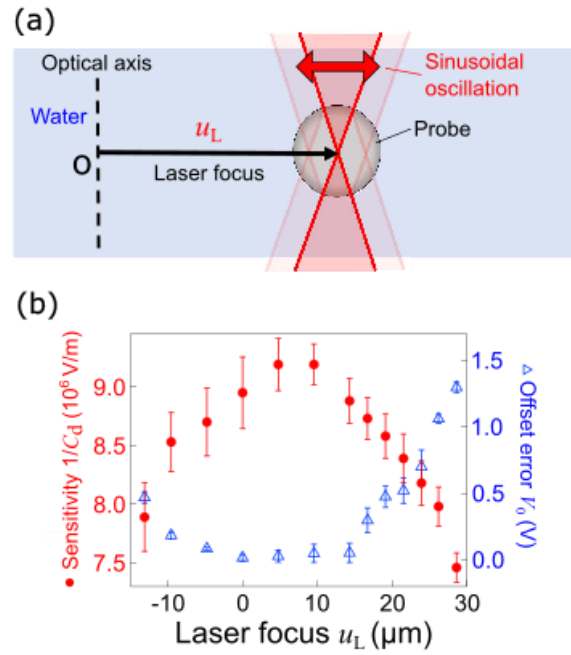
FIG. 4. (a) A schematic illustration of the experiment to evaluate the dependence of sensitivity $1/C_d$ and offset error V_0 on the focus position (u_L). The melamine particle with a diameter of 1 µm was dispersed in water, and trapped by the oscillating laser ($\lambda = 1064$ nm). By analyzing the QPD output, $1/C_d$ and V_0 were obtained as a function of u_L. (b) Dependence of $1/C_d$ (*red circles*) and V_0 (*blue open triangles*) on u_L. $1/C_d$ decreased and V_0 increased when the position of the laser focus was deviated from the center of the optical axis. At the largest u_L in this measurement ($u_L = 28.6$ µm), $V_0 \simeq 1.3$ V corresponded to 0.2 µm when calibrated. The position with the highest sensitivity was shifted from the center of the optical axis probably because the center of the operating range of the AOD-controlled laser did not match the optical axis.

the probe laser is fixed. When the probe was moved more

than 10 μm, $1/C_d$ and V_0 commonly alter by the amount similar to those observed here. The accuracy of particle tracking during the force feedback thus depends on the movement of the probe laser that follows the probe fluctuation. When a probe particle fluctuates vigorously, dual-feedback technique should be used to keep the laser movement within a certain limit that should be determined by the accuracy required for the measurement. Because the feedback-controlled stage tracks the slow and large movement of the probe particle, the AOD-controlled laser is kept close to the optical axis. Therefore, the dual-feedback technique is necessary to perform BFPI accurately when a probe particle vigorously fluctuates or drifts in samples driven out of equilibrium.

References

[1] B. Alberts, *Essential cell biology*, Fourth edition. edn.

[2] M. Atakhorrami, G. H. Koenderink, J. F. Palierne, F. C. MacKintosh, and C. F. Schmidt, Phys Rev Lett **112**, 088101 (2014).

[3] D. W. Frederiksen and L. W. Cunningham, methods enzymol **85** (1982).

[4] J. Liu, M. L. Gardel, K. Kroy, E. Frey, B. D. Hoffman, J. C. Crocker, A. R. Bausch, and D. A. Weitz, Phys Rev Lett **96**, 118104 (2006).

[5] B. Schnurr, F. Gittes, F. C. MacKintosh, and C. F. Schmidt, Macromolecules **30**, 7781 (1997).

[6] I. Y. Wong, M. L. Gardel, D. R. Reichman, E. R. Weeks, M. T. Valentine, A. R. Bausch, and D. A. Weitz, Phys Rev Lett **92**, 178101 (2004).

[7] M. Tassieri, R. M. L. Evans, L. Barbu-Tudoran, G. N. Khaname, J. Trinick, and T. A. Waigh, Phys Rev Lett **101** (2008).

[8] F. Gittes and C. F. Schmidt, Method Cell Biol **55**, 129 (1998).

[9] T. G. Mason, K. Ganesan, J. H. vanZanten, D. Wirtz, and S. C. Kuo, Phys Rev Lett **79**, 3282 (1997).

[10] D. Mizuno, D. A. Head, F. C. MacKintosh, and C. F. Schmidt, Macromolecules **41**, 7194 (2008).

[11] L. A. Hough and H. D. Ou-Yang, Phys Rev E **65**, 021906 (2002).

[12] D. Mizuno, Y. Kimura, and R. Hayakawa, Phys Rev Lett **87**, 088104 (2001).

[13] R. M. L. Evans, M. Tassieri, D. Auhl, and T. A. Waigh, Physical Review E **80** (2009).

[14] F. Gittes, B. Schnurr, P. D. Olmsted, F. C. MacKintosh, and C. F. Schmidt, Phys Rev Lett **79**, 3286 (1997).

[15] D. Mizuno, Y. Kimura, and R. Hayakawa, Langmuir **16**, 9547 (2000).

[16] D. Mizuno, C. Tardin, C. F. Schmidt, and F. C. Mackintosh, Science **315**, 370 (2007).

[17] S. Jabbari-Farouji, D. Mizuno, D. Derks, G. H. Wegdam, F. C. MacKintosh, C. F. Schmidt, and D. Bonn, Epl-Europhys Lett **84**, 20006 (2008).

[18] C. D. Chapman and R. M. Robertson-Anderson, Phys Rev Lett **113**, 098303 (2014).

[19] M. Khan, K. Regan, and R. M. Robertson-Anderson, Phys Rev Lett **123**, 038001 (2019).

[20] L. G. Wilson, A. W. Harrison, W. C. K. Poon, and A. M. Puertas, Epl-Europhys Lett **93**, 58007 (2011).

[21] M. Doi and S. F. Edwards, *The theory of polymer dynamics* (Clarendon Press; Oxford University Press, Oxford, New York, 1986).

[22] B. Wang, S. M. Anthony, S. C. Bae, and S. Granick, Proc Natl Acad Sci U S A **106**, 15160 (2009).

[23] B. Wang, J. Kuo, S. C. Bae, and S. Granick, Nat Mater **11**, 481 (2012).

[24] T. Toyota, D. A. Head, C. F. Schmidt, and D. Mizuno, Soft Matter **7**, 3234 (2011).

[25] F. Gittes and C. F. Schmidt, Opt Lett **23**, 7 (1998).

[26] M. Atakhorrami, J. I. Sulkowska, K. M. Addas, G. H. Koenderink, J. X. Tang, A. J. Levine, F. C. Mackintosh, and C. F. Schmidt, Phys Rev E **73**, 061501 (2006).

[27] K. Nishizawa, M. Bremerich, H. Ayade, C. F. Schmidt, T. Ariga, and D. Mizuno, Sci Adv **3**, e1700318 (2017).

[28] Y. Sugino, M. Ikenaga, and D. Mizuno, Appl Sci-Basel **10**, 4970 (2020).

[29] T. Kurihara, M. Aridome, H. Ayade, I. Zaid, and D. Mizuno, Phys Rev E **95**, 030601 (2017).

[30]   D. A. Head, E. Ikebe, A. Nakamasu, P. Zhang, L. G. Villaruz, S. Kinoshita, S. Ando, and D. Mizuno, Phys Rev E **89**, 042711 (2014).

[31]   M. L. Gardel, J. H. Shin, F. C. MacKintosh, L. Mahadevan, P. Matsudaira, and D. A. Weitz, Science **304**, 1301 (2004).

[32]   T. Ariga, M. Tomishige, and D. Mizuno, Phys Rev Lett **121**, 218101 (2018).

[33]   J. W. J. Kerssemakers, E. L. Munteanu, L. Laan, T. L. Noetzel, M. E. Janson, and M. Dogterom, Nature **442**, 709 (2006).

[34]   H. Akaike, in *Selected papers of hirotugu akaike* (Springer, 1998), pp. 199.

[35]   K. P. Burnham, (No Title) (2002).

[36]   F. C. MacKintosh, J. Kas, and P. A. Janmey, Phys Rev Lett **75**, 4425 (1995).

[37]   D. C. Morse, Macromolecules **31**, 7030 (1998).

[38]   C. P. Broedersz and F. C. MacKintosh, Reviews of Modern Physics **86**, 995 (2014).

[39]   B. Gurmessa, S. Ricketts, and R. M. Robertson-Anderson, Biophysical journal **113**, 1540 (2017).

[40]   M. E. Dwyer, R. M. Robertson-Anderson, and B. J. Gurmessa, Polymers **14**, 4980 (2022).

[41]   N. Honda, K. Shiraki, F. Van Esterik, S. Inokuchi, H. Ebata, and D. Mizuno, New J Phys **24**, 053031 (2022).

[42]   D. A. Head and D. Mizuno, Phys Rev E **88**, 022717 (2013).

[43]   R. Metzler and J. Klafter, Phys Rep **339**, 1 (2000).

[44]   C. Monthus and J. P. Bouchaud, J Phys a-Math Gen **29**, 3847 (1996).

[45]   E. M. Bertin and J. P. Bouchaud, Phys Rev E **67**, 026128 (2003).

[46]   J. P. Bouchaud, J Phys I **2**, 1705 (1992).

[47]   P. Sollich, F. Lequeux, P. Hebraud, and M. E. Cates, Phys Rev Lett **78**, 2020 (1997).

[48]   N. Yamamoto, M. Ichikawa, and Y. Kimura, Phys Rev E **82**, 021506 (2010).

[49]   C. P. Brangwynne, G. H. Koenderink, F. C. Mackintosh, and D. A. Weitz, Phys Rev Lett **100**, 118104 (2008).

[50]   K. Nishizawa, K. Fujiwara, M. Ikenaga, N. Nakajo, M. Yanagisawa, and D. Mizuno, Sci Rep-Uk **7**, 15143 (2017).

[51]   D. Humphrey, C. Duggan, D. Saha, D. Smith, and J. Kas, Nature **416**, 413 (2002).